Journal of Nuclear Medicine, published on July 25, 2013 as doi:10.2967/jnumed.113.120659

Quantification of Cardiac Sympathetic Nerve Density with *N*-^{11}C-Guanyl-*meta*-Octopamine and Tracer Kinetic Analysis

David M. Raffel, Robert A. Koeppe, Yong-Woon Jung, Guie Gu, Keun Sam Jang, Phillip S. Sherman, and Carole A. Quesada

Division of Nuclear Medicine, Department of Radiology, University of Michigan Medical School, Ann Arbor, Michigan

Most cardiac sympathetic nerve radiotracers are substrates of the norepinephrine transporter (NET). Existing tracers such as ^{123}I-metaiodobenzylguanidine (^{123}I-MIBG) and ^{11}C-(–)-*meta*-hydroxyephedrine (^{11}C-HED) are flow-limited tracers because of their rapid NET transport rates. This prevents successful application of kinetic analysis techniques and causes semiquantitative measures of tracer retention to be insensitive to mild-to-moderate nerve losses. *N*-^{11}C-guanyl-(–)-*meta*-octopamine (^{11}C-GMO) has a much slower NET transport rate and is trapped in storage vesicles. The goal of this study was to determine whether analyses of ^{11}C-GMO kinetics could provide robust and sensitive measures of regional cardiac sympathetic nerve densities. **Methods:** PET studies were performed in a rhesus macaque monkey under control conditions or after intravenous infusion of the NET inhibitor desipramine (DMI). Five desipramine dose levels were used to establish a range of available cardiac NET levels. Compartmental modeling of ^{11}C-GMO kinetics yielded estimates of the rate constants K_1 (mL/min/g), k_2 (min^{-1}), and k_3 (min^{-1}). These values were used to calculate a net uptake rate constant K_i (mL/min/g) = $(K_1k_3)/(k_2 + k_3)$. In addition, Patlak graphical analyses of ^{11}C-GMO kinetics yielded Patlak slopes K_p (mL/min/g), which represent alternative measurements of the net uptake rate constant K_i. ^{11}C-GMO kinetics in isolated rat hearts were also measured for comparison with other tracers. **Results:** In isolated rat hearts, the neuronal uptake rate of ^{11}C-GMO was 8 times slower than ^{11}C-HED and 12 times slower than ^{11}C-MIBG. ^{11}C-GMO also had a long neuronal retention time (>200 h). Compartmental modeling of ^{11}C-GMO kinetics in the monkey heart proved stable under all conditions. Calculated net uptake rate constants K_i tracked desipramine-induced reductions of available NET in a dose-dependent manner, with a half maximal inhibitory concentration (IC_{50}) of 0.087 ± 0.012 mg of desipramine per kilogram. Patlak analysis provided highly linear Patlak plots, and the Patlak slopes K_p also declined in a dose-dependent manner (IC_{50} = 0.068 ± 0.010 mg of desipramine per kilogram). **Conclusion:** Compartmental modeling and Patlak analysis of ^{11}C-GMO kinetics each provided quantitative parameters that accurately tracked changes in cardiac NET levels. These results strongly suggest that PET studies with ^{11}C-GMO can provide robust and sensitive quantitative measures of regional cardiac sympathetic nerve densities in human hearts.

Key Words: norepinephrine transporter; hydroxyephedrine; metaiodobenzylguanidine; positron emission tomography

J Nucl Med 2013; 54:1–8
DOI: 10.2967/jnumed.113.120659

Received Jan. 28, 2013; revision accepted Apr. 4, 2013.

For correspondence or reprints contact: David M. Raffel, Department of Radiology, Division of Nuclear Medicine, 2276 Medical Sciences I, 1301 Catherine St., SPC-5610, Ann Arbor, MI 48109.

E-mail: raffel@umich.edu

Published online ■■■■■■■■■■■■.

It has been more than 30 y since radioiodinated metaiodobenzylguanidine (MIBG) was first introduced for scintigraphic imaging of cardiac sympathetic innervation (*1*). Since then, several other radiotracers, including ^{11}C-(–)-*meta*-hydroxyephedrine (^{11}C-HED) and ^{11}C-(–)-epinephrine (^{11}C-EPI), have been developed to assess cardiac sympathetic nerve integrity with PET (*2*). Clinical studies with these tracers have made significant contributions to our understanding of cardiac sympathetic dysfunction in many diseases (*3*). In addition, recent studies point to an emerging role for cardiac neuronal imaging in the identification of heart failure patients at high risk for sudden cardiac death (*4*).

As structural analogs of the neurotransmitter norepinephrine, these tracers are actively transported into neurons by the norepinephrine transporter (NET) and stored in norepinephrine storage vesicles by the vesicular monoamine transporter 2. Retention of a tracer in vesicles is dependent on its structure—highly polar compounds such as ^{11}C-EPI have long vesicular retention times, whereas more lipophilic compounds such as ^{11}C-HED diffuse out of vesicles fairly quickly (*5*).

This approach to imaging sympathetic neurons has proven to be effective, providing high-quality cardiac images that roughly map the regional distribution of functional nerve terminals. However, a major limitation of the current generation of tracers is that their neuronal uptake rates, mediated by NET transport, are too rapid to allow accurate quantification of regional nerve densities. Rapid NET transport causes the net neuronal uptake of the tracers to be rate-limited by delivery from plasma to interstitium, rather than by NET-mediated neuronal uptake. Because delivery is governed primarily by perfusion, these are flow-limited tracers. As a result, their myocardial kinetics cannot be successfully analyzed using standard kinetic analysis methodology. The inability to obtain quantitative measures using kinetic analysis methods forces the use of semiquantitative measures of tracer retention as surrogate measures of nerve density, including the heart-to-mediastinum ratio for MIBG and the retention index for ^{11}C-HED. However, because of the flow-limited uptake of the tracers, retention measures are insensitive to low-to-moderate levels of regional denervation and decline only when nerve losses become fairly severe (*6*).

To overcome these limitations, our laboratory has been developing new tracers with more optimal kinetics for quantifying regional nerve density. Our goal was to develop a tracer with 2 specific kinetic characteristics. First, a slower NET transport rate was needed, making this the rate-limiting step in the neuronal uptake of the tracer. Second, efficient trapping inside storage vesicles was desired, leading to long neuronal retention times

[Fig. 1] (Fig. 1A). We hypothesized that a tracer with these properties could have its myocardial kinetics analyzed with a simple compartmental model in which the neurons act kinetically as a single irreversible compartment (Fig. 1B). In addition, these properties would allow the application of the Patlak graphical method for estimating the tracer's net neuronal uptake rate (*7*).

To this end, our studies of a series of ^{11}C-labeled phenethylguanidines identified *N*-^{11}C-guanyl-(–)-*meta*-octopamine (^{11}C-[Fig. 2] GMO, Fig. 2) as a promising tracer exhibiting the 2 targeted properties (*8*). The goal of the current study was to test our hypothesis that ^{11}C-GMO would exhibit myocardial kinetics that could be successfully analyzed with tracer kinetic techniques. We also evaluated the ability of quantitative measures from analyses of ^{11}C-GMO kinetics to track declines in available NET densities, induced pharmacologically with the potent NET inhibitor desipramine.

MATERIALS AND METHODS

Radiochemistry

^{11}C-GMO and ^{11}C-MIBG were synthesized as previously described (*8*). ^{11}C-HED was prepared using previously published methods (*9*). Specific activities for these compounds were 18.5–55.0 TBq/mmol. ^{18}F-FDG was prepared as previously described (*10*).

Animal Care. The care of all animals used in this study was done in accordance with the Animal Welfare Act and the National Institutes of Health's *Guide for the Care and Use of Laboratory Animals* (*11*). Animal protocols were approved by the University Committee on Use and Care of Animals at the University of Michigan.

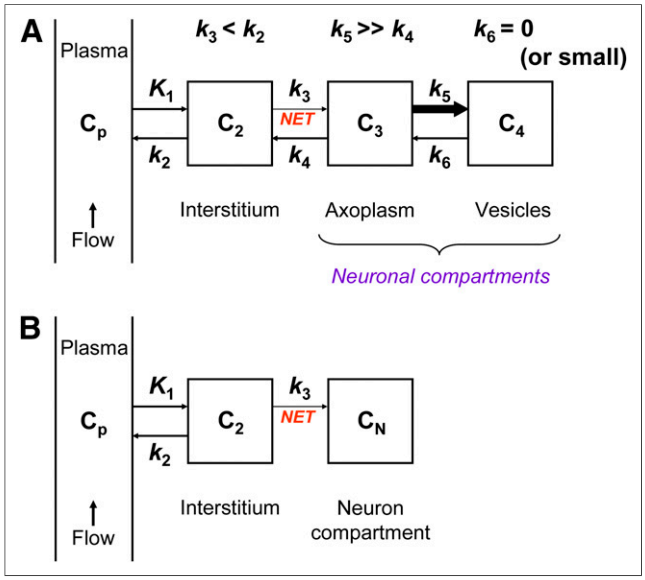

RGB

FIGURE 1. (A) Comprehensive compartmental model of sympathetic nerve radiotracer with optimal kinetic properties. Arrow thicknesses are drawn in approximate proportion to magnitude of rate constants. If NET transport rate of tracer (k_3) is less than efflux rate from interstitium back into plasma (k_2), this prevents tissue uptake of tracer from being flow-limited. Furthermore, if vesicular storage rate (k_5) is rapid relative to efflux from neuronal axoplasm (k_4), and tracer is effectively trapped in vesicles (k_6 = 0 or small), 2 neuronal compartments kinetically behave as single trapping compartment. This allows use of simplified compartmental model (B) for quantitative analysis of kinetic data from PET studies.

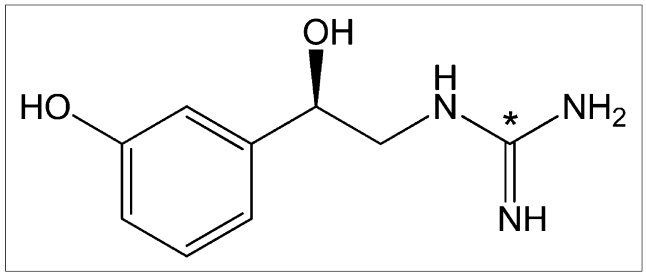

FIGURE 2. Structure of ^{11}C-GMO. ^{11}C label is incorporated into guanidine group (*).

Isolated Rat Heart Studies

Kinetic studies of the neuronal uptake and retention of ^{11}C-GMO, ^{11}C-HED, and ^{11}C-MIBG were performed with an isolated working rat heart system (*8,12*) under moderate workload conditions (10 cm H_2O preload, 100 cm H_2O afterload). For comparison, a study with ^{18}F-FDG was performed under identical conditions except that the perfusate glucose concentration was changed from 5 to 10 mM. A 10-min constant infusion of tracer at low concentrations was performed to measure neuronal uptake rates. The heart was then switched to a second perfusion circuit with normal perfusate for 120 min to study tracer clearance from sympathetic nerve terminals. Coincidence counting rate data (cps/heart) from 2 opposing 5.1 × 5.1 cm cesium fluoride detectors were corrected for random coincidences and normalized to the activity concentration in perfusate (cps/mL perfusate) and the heart's wet mass (g wet/heart) to express heart uptake of tracer as an apparent distribution volume (mL perfusate/g wet). Neuronal uptake rates K_{up} (mL perfusate/min/g wet) were determined as the linear slope of the apparent distribution volume data between 1 and 4 min of the constant infusion study. Clearance kinetics were fit to multiple exponential decay processes to characterize clearance rates. For the nerve tracers, 54 μM corticosterone was added to perfusate to block extraneuronal uptake (uptake-2) into myocytes (*13*), which competes with neuronal uptake (uptake-1) in rat hearts but is absent in nonhuman primate and human hearts (*6*).

PET Imaging

PET imaging was performed using a Concorde Microsystems microPET P4 primate scanner (19-cm field of view, 7.8-cm axial extent, 1.75-mm intrinsic spatial resolution, and 2.25% peak system sensitivity) (*14*). After the monkey was anesthetized, a percutaneous angiocather was placed in the saphenous vein of each leg (1 for tracer injection, 1 for blood sampling). Heart rate (bpm), blood oxygen saturation levels (SpO_2), and body temperature were monitored continuously (V3404P; SurgiVet). A transmission scan was acquired using a rotating ^{68}Ge/^{68}Ga rod source for attenuation corrections. Dynamic PET data were acquired in list-mode for 60 min after ^{11}C-GMO injection (24–44 MBq/kg). List-mode emission data were rebinned into a 24-frame dynamic sequence (12 × 10, 2 × 30, 2 × 60, 2 × 150, 2 × 300, and 4 × 600 s). Rebinned emission data were corrected for attenuation and scatter, and transaxial images were reconstructed using maximum a posteriori reconstruction (*15*), an iterative method that accounts for the detector point spread function in the model of the system.

Radiometabolite Analyses

Before imaging, a blood sample (1.5–2.0 mL) was drawn, and 3.7 MBq of ^{11}C-GMO were added. This was incubated at 37°C for 60–70 min to determine tracer stability in blood. During the PET scan, 4 venous blood samples (1.5–2.0 mL) were drawn at 5, 15, 30, and 55 min to assess radiometabolites in plasma and partitioning of

jnm120659-pm ■ 7/22/13

^{11}C-GMO between plasma and red blood cells (RBCs). Blood samples were centrifuged for 1 min at 12,000*g* to separate plasma and RBCs. Plasma was deproteinized by adding perchloric acid ($HClO_4$; final concentration, 0.4N) and centrifuging for 5 min at 12,000*g*. The supernatant was neutralized with KOH (pH 7.0–7.5), filtered twice (0.22-μm filters; Millipore Millex/GS), and analyzed by high-performance liquid chromatography (HPLC) (10μ Hydro-RP column [Syergi]; 4.6 × 250 mm, 60 mM sodium phosphate buffer, pH 5.4, with 3% ethanol; flow rate, 1.0 mL/min) and radiation detection (905-4 NaI (Tl) detector; Ortec). The sample spiked with ^{11}C-GMO was processed in the same way. Aliquots (0.1 mL) of whole blood, plasma, final supernatant, and pellets were counted in a γ-counter. Count data (decay-corrected) were used to determine the relative concentrations of ^{11}C-GMO in plasma and whole blood (C_p/C_{wb}). HPLC and radiation detection data (decay-corrected) were processed for peak analysis (ACD/ChromProcessor, version 10; ACD Inc.) to determine the percentage of activity associated with intact ^{11}C-GMO (f_{intact}). A mathematic function describing the time course of the metabolic breakdown of ^{11}C-GMO in plasma, $f_{intact}(t)$, was obtained by nonlinear regression analysis (Prism 3.0; GraphPad Software).

Tracer Kinetic Analyses

Summed images of the final 4 PET frames were used to draw regions of interest on the myocardial wall and on the blood pool in the basal left ventricular chamber to extract time–activity curves for myocardial tissue $C_t(t)$ and whole blood $C_{wb}(t)$. The plasma concentration of intact ^{11}C-GMO versus time, $C_p(t)$, was estimated by multiplying $C_{wb}(t)$ by the metabolic breakdown function, $f_{intact}(t)$, and the mean ratio of activity concentrations in plasma and whole blood, C_p/C_{wb}. Thus, $C_p(t) = C_{wb}(t) \cdot f_{intact}(t) \cdot [C_p/C_{wb}]$. The plasma time–activity curve, $C_p(t)$, was used with the tissue time–activity curve, $C_t(t)$, for compartmental modeling. Nonlinear regression analysis with the simplified compartmental model (Fig. 1B) provided estimates of the rate constants K_1 (mL/min/g), k_2 (min^{-1}), k_3 (min^{-1}), and a blood volume fraction, *BV* (dimensionless), using in-house analysis software. Rate constant estimates were used to calculate a net uptake rate constant K_i (mL/min/g) = $(K_1k_3)/(k_2 + k_3)$, which reflects the rate of ^{11}C-GMO accumulation into nerve terminals. Tissue and plasma kinetics of ^{11}C-GMO were also analyzed using Patlak graphical analysis (*7*). After construction of a Patlak plot, the last 9 points of the plot were analyzed with linear regression to determine the Patlak slope, K_p (mL/min/g). Under ideal conditions, the Patlak slope, K_p, is a direct measure of the net uptake rate constant, K_i, and thus for the model structure shown in Figure 1B is also equal to $(K_1k_3)/(k_2 + k_3)$.

Control and Pharmacologic Blocking Studies

In addition to control conditions ($n = 4$), NET blocking studies were performed with the NET inhibitor desipramine. The goal of these studies was to assess the ability of the quantitative parameters from kinetic analyses to track progressively lower cardiac NET densities induced pharmacologically by increasing desipramine doses. All studies were performed in the same monkey to minimize biologic variation between studies and to make initial assessments of the reproducibility of quantitative measures of NET density. The desipramine dose (dissolved into 2.0 mL of sterile saline) was infused intravenously over 20 min using an infusion pump. ^{11}C-GMO was injected 10 min after the end of the desipramine infusion. Desipramine doses used were 0.010 mg/kg ($n = 2$), 0.0316 mg/kg ($n = 2$), 0.10 mg/kg ($n = 2$), 0.316 mg/kg ($n = 1$), and 1.0 mg/kg ($n = 1$). The measured kinetic parameters K_i from compartmental modeling and K_p values from Patlak analysis, as a function of desipramine dose, were fit to a sigmoidal dose–response model with variable slope using nonlinear regression (Prism 3.0; GraphPad Software).

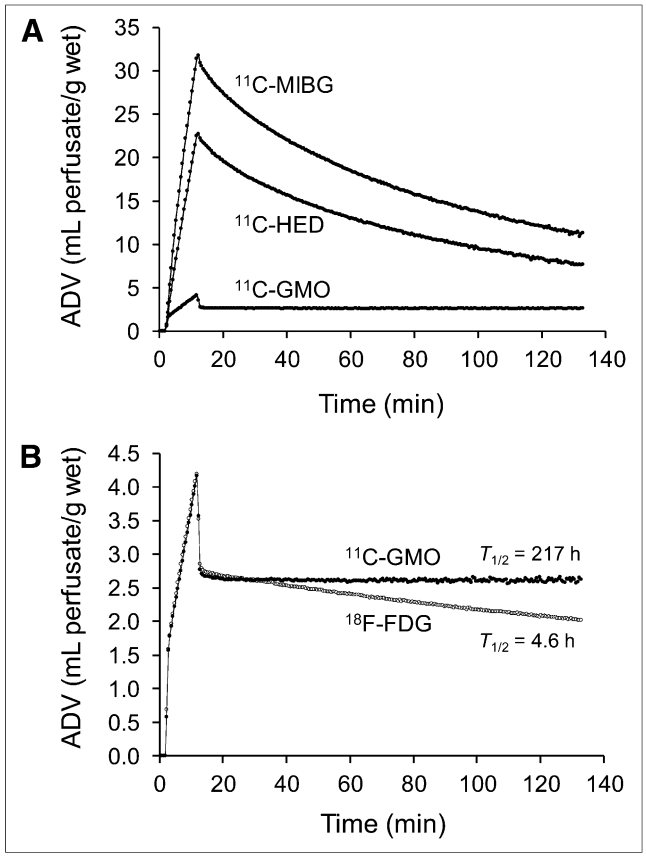

FIGURE 3. (A) Kinetics of ^{11}C-MIBG, ^{11}C-HED, and ^{11}C-GMO in isolated working rat hearts. In each case, 10-min constant infusion of tracer was performed to measure neuronal uptake rates (K_{up}; mL/min/g wet), then heart switched to normal heart perfusate to study efflux rates from neuronal spaces. (B) For comparison, isolated rat heart kinetics of ^{11}C-GMO are shown along with those of ^{18}F-FDG. Note different *y*-axis scales used in A and B.

RESULTS

Isolated Rat Heart Studies

The neuronal uptake and retention kinetics of ^{11}C-GMO in the isolated rat heart are shown in Figure 3A, in comparison to those of ^{11}C-MIBG and ^{11}C-HED. ^{11}C-GMO possesses a much slower neuronal uptake rate (K_{up}) than the other 2 tracers (Table 1), about 8 times slower than ^{11}C-HED and 12 times slower than ^{11}C-MIBG. ^{11}C-GMO also has a much longer neuronal retention time than ^{11}C-MIBG and ^{11}C-HED (Table 1). A slower neuronal uptake rate and a long retention time are the 2 kinetic properties we hypothesized a nerve tracer would require for its kinetics to be analyzed successfully with tracer kinetic techniques. It is also in-

[**Fig. 3**]

[**Table 1**]

TABLE 1
Uptake Rates and Major Clearance Half-Times in Isolated Rat Hearts, as Shown in Figure 3

Tracer	K_{up} (mL/min/g)	Major clearance half-time (h)
^{11}C-MIBG	3.65	2.1
^{11}C-HED	2.35	1.1
^{11}C-GMO	0.30	217
^{18}F-FDG	0.31	4.6

jnm120659-pm ■ 7/22/13

teresting to compare the kinetics of ^{11}C-GMO with those of the well-established cardiac tracer ^{18}F-FDG (10 mM glucose, no insulin) in this model (Fig. 3B). The uptake kinetics of the 2 tracers are almost identical, whereas ^{18}F-FDG clears from the myocardium with a major half-time of 4.6 h, compared with a neuronal clearance half-time of more than 200 h for ^{11}C-GMO (Table 1). Because coronary flow rates are more than 10 times physiologic levels in this system, tracers diffusing from tissue spaces tend to be cleared from the isolated heart at faster rates than would be seen in vivo. Thus, storage of ^{11}C-GMO inside vesicles is an effective trapping mechanism leading to extremely long neuronal retention times.

^{11}C-GMO Metabolism

In monkey studies, ^{11}C-GMO was metabolized into 1 major and 2 minor metabolites, all of which were more polar than the parent compound (Fig. 4A). The half-time for the metabolic breakdown of ^{11}C-GMO averaged 16.0 ± 3.0 min (range, 11.0–22.5 min). In most cases, the fraction of plasma activity associated with intact ^{11}C-GMO versus time was fit to the following function (Fig. 4B):

[Fig. 4]

$$f_{\text{intact}}(t) = \text{span} \times \left(\frac{B^n}{t^n + B^n} \right) + \text{plateau}. \qquad \text{Eq. 1}$$

For the study using a desipramine dose of 1.0 mg/kg, it was necessary to use an alternative function:

$$f_{\text{intact}}(t) = \text{span} \times \left(\frac{Ue^{-At} - Ae^{-Ut}}{U - A} \right) + \text{plateau}. \qquad \text{Eq. 2}$$

The fitted curve for $f_{\text{intact}}(t)$ was used in preparing the input function, $C_p(t)$, for kinetic analyses. HPLC analyses of blood samples spiked with ^{11}C-GMO showed only the parent compound, indicating that it is stable in blood and plasma. Similar to ^{123}I-MIBG and ^{11}C-HED, ^{11}C-GMO is metabolically stable inside neurons. The guanidine group in the side chain of ^{11}C-GMO prevents metabolism by neuronal enzymes such as monoamine oxidase, although some phenethylguanidines are reversible monoamine oxidase inhibitors (*16*). ^{11}C-GMO lacks the catechol structure of catecholamines such as norepinephrine, so it is not metabolized by catechol-*O*-methyl-transferase.

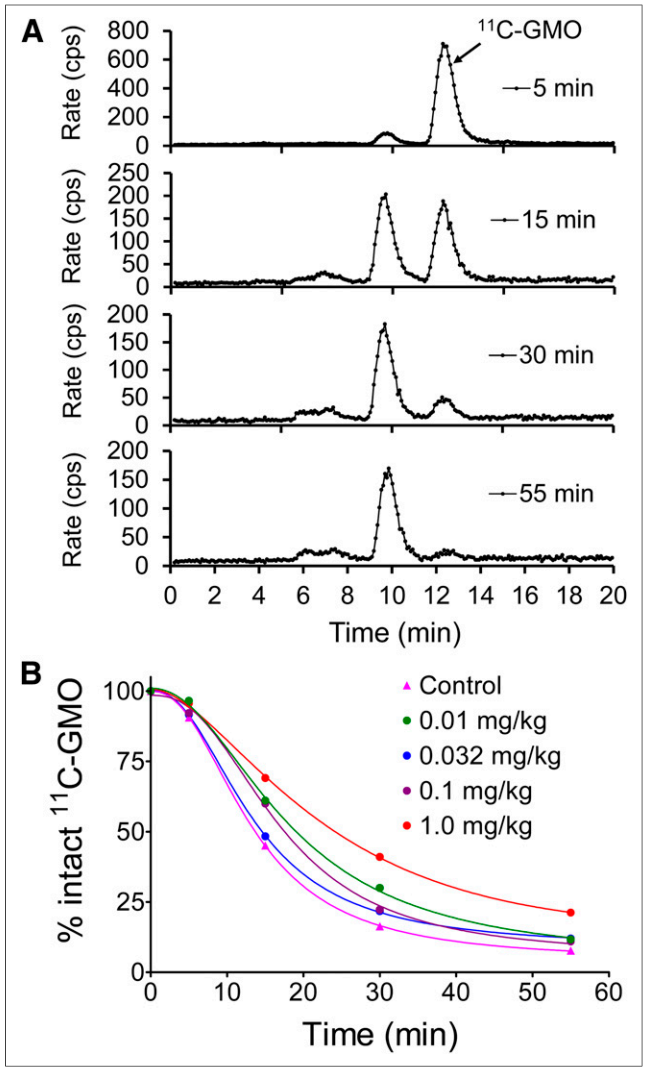

RGB

FIGURE 4. (A) Reversed-phase HPLC and radiodetection analysis of radiometabolite formation in plasma. (B) Fraction of activity associated with intact ^{11}C-GMO was determined for each sample, and percentage intact vs. time data fit to mathematic function to characterize metabolic breakdown of ^{11}C-GMO.

^{11}C-GMO Partitioning in Blood

Analysis of ^{11}C-GMO concentrations in whole blood, plasma, and RBCs demonstrated that ^{11}C-GMO stays primarily in plasma, with little uptake into RBCs. The ratio of plasma and whole-blood activity concentrations, $C_p(t)/C_{wb}(t)$, tended to be constant throughout the PET study. For all of the blood samples drawn during PET scanning, the average ratio was 1.47 ± 0.08. Similarly, for all spiked blood samples, the mean ratio was 1.41 ± 0.07. Desipramine block of cardiac NET had no effect on the blood partitioning of ^{11}C-GMO. Blood partitioning data for each study was used in the preparation of input functions for kinetic analyses.

Effects of Desipramine Infusion and ^{11}C-GMO Injection

Body temperature and SpO_2 levels were stable during all studies. For desipramine levels at 0.10 mg/kg and below, desipramine infusion caused no change in heart rate. However, for desipramine doses of 0.316 and 1.0 mg/kg, starting 3 min into the desipramine infusion, heart rate steadily rose from a baseline of around 100 bpm up to 122–125 bpm at 1 min after desipramine infusion. Heart rate then slowly declined 4–8 bpm over the next 60 min. Intravenous injection of ^{11}C-GMO had no effect on heart rate, with only a transient increase of 1–2 bpm for 1 min observed during the desipramine study using a dose of 0.316 mg/kg.

Imaging Properties

Representative transaxial PET images from a control study and progressively higher desipramine block studies are shown in Figure 5. The images clearly show a desipramine dose–dependent decline in the cardiac retention of ^{11}C-GMO. In controls, heart-to-blood ratios of 3.01 ± 0.18 and heart-to-liver ratios of 0.89 ± 0.24 were seen in the final image (n = 4). If the relatively high liver uptake of ^{11}C-GMO also occurs in human subjects, this could be a minor drawback because the liver is often close to inferior or inferoseptal segments of the left ventricle, leading to some spillover of counts from liver into these segments.

[Fig. 5]

jnm120659-pm ■ 7/22/13

RGB

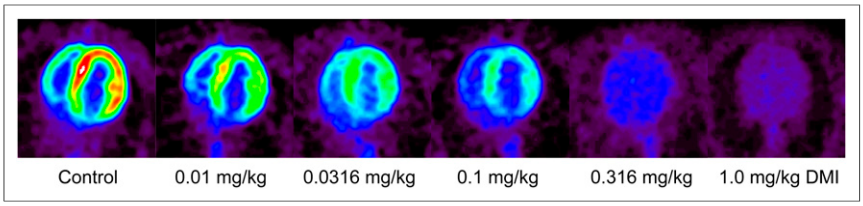

FIGURE 5. Representative transaxial small-animal PET images of cardiac ^{11}C-GMO retention. Shown are summed images (final 4 dynamic frames) for control study (far left) and for blocking studies with progressively higher doses of NET inhibitor desipramine.

Kinetic Analysis: Compartmental Modeling

Compartmental modeling of ^{11}C-GMO kinetics proved to be robust in the sense that the nonlinear regression algorithm converged in a few iterations to a single global minimum. Myocardial time–activity curves and corresponding compartmental model fits for a control study and 3 of the desipramine blocking doses are presented in Figures 6A–6D. Model parameter estimates for all studies are given in Table 2. Parameter estimates were fairly consistent within groups, but values of k_3, which ideally should reflect cardiac NET density, did not decrease with increasing desipramine doses. However, the net uptake rate constant K_i calculated from the combination of estimated rate constants $(K_1k_3)/(k_2 + k_3)$ did provide a quantitative measure that sensitively tracked reductions in available cardiac NET in a desipramine dose–dependent manner (Table 2; Fig. 6E). Declines in K_i values (Y) versus increasing desipramine doses were well described by a sigmoidal dose–response model with variable Hill slope (n_H), where X = log [desipramine dose]:

$$Y = \frac{Y_{max}}{1 + 10^{[\log(IC_{50}) - X] \times n_H}}. \quad \text{Eq. 3}$$

For the K_i data, nonlinear regression analysis yielded parameter estimates of IC_{50} = 0.087 ± 0.012 mg/kg desipramine, Hill slope n_H = –0.70 ± 0.07, and a maximum net uptake rate constant Y_{max} = 0.130 ± 0.003 mL/min/g (r^2 = 0.99). Because the Hill slope is less than –1.0, this indicates that the dose–response curve is more shallow than the standard 1-site competition dose–response curve used frequently for in vitro competitive displacement assays. The observation that estimates of the individual model parameters K_1, k_2, k_3, and BV were variable and that k_3 estimates alone did not serve as the index of NET density was not unexpected, because a similar situation exists for analyses of ^{18}F-FDG kinetics in assessments of cardiac glucose utilization (*17*).

Kinetic Analysis: Patlak Graphical Analysis

Patlak analysis of ^{11}C-GMO kinetics provided highly linear Patlak plots under all experimental conditions, with linear correlation coefficients $r > 0.99$ in all cases (Fig. 7A). Measured Patlak slopes K_p (mL/min/g) are shown in Table 2. Similar to the K_i values from compartmental modeling, the measured Patlak slopes K_p declined along a sigmoidal dose–response curve (Fig. 7B) with increasing doses of desipramine: IC_{50} = 0.068 ± 0.010 mg/kg desipramine, Hill slope n_H = –0.54 ± 0.05, and a maximum Patlak slope Y_{max} = 0.104 ± 0.002 mL/min/g (r^2 = 0.99). There was a strong linear correlation between the measured Patlak slopes and the calculated K_i values from compartmental modeling: $K_p = (0.757)K_i + 0.001$, with linear correlation coefficient r = 0.99 (data not shown).

DISCUSSION

This study was designed to test whether quantitative measurements derived from analyses of myocardial ^{11}C-GMO kinetics are capable of sensitively tracking cardiac sympathetic nerve densities over the full dynamic range seen in normal subjects and in patients with heart disease. The experimental approach used was to pharmacologically induce varying degrees of cardiac NET inhibition using the NET inhibitor desipramine. Our findings demonstrated that 2 measures of the net uptake rate constant K_i—obtained either by calculation from compartmental modeling results or as the Patlak slope K_p from Patlak graphical analysis—each appear to serve as robust and reproducible measures of regional cardiac sympathetic nerve density. To the best of our knowledge, ^{11}C-GMO is the first sympathetic nerve radiotracer to possess myocardial kinetics that can

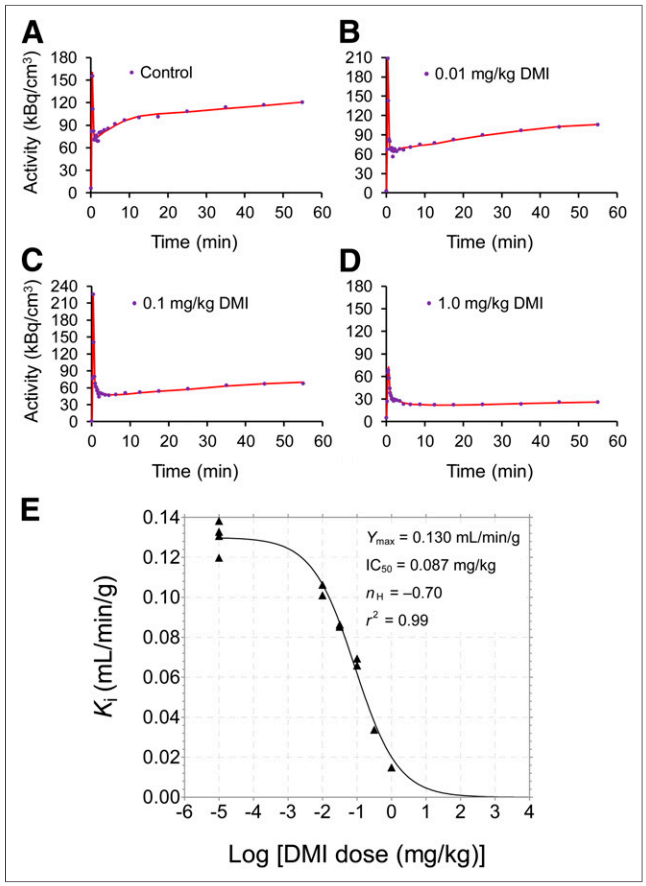

RGB

FIGURE 6. Compartmental modeling of ^{11}C-GMO kinetics using simplified model shown in Figure 1B. Myocardial ^{11}C-GMO kinetics (blue dots) and corresponding compartmental model fits (red lines) are shown for control study (A) and 3 different desipramine blocking doses (B–D). (E) Relationship between net uptake rate constants K_i (mL/min/g) calculated from compartmental model parameter estimates and log [desipramine dose (mg/kg)]. Decline in K_i values was well described by sigmoidal dose–response curve with variable Hill slope (n_H). Estimated parameter values for dose–response curve fit are shown.

jnm120659-pm ■ 7/22/13

TABLE 2
Results from Compartmental Modeling and Patlak Analysis of ^{11}C-GMO Kinetics

Study	Compartmental modeling					Patlak analysis, K_p (mL/min/g)
	K_1 (mL/min/g)	k_2 (min^{-1})	k_3 (min^{-1})	*BV*	K_i (mL/min/g)	
Control						
A	0.392	0.145	0.074	0.322	0.133	0.104
B	0.345	0.123	0.082	0.283	0.138	0.111
C	0.306	0.082	0.061	0.278	0.131	0.102
D	0.282	0.117	0.087	0.252	0.120	0.099
Desipramine dose						
0.01 mg/kg						
A	0.245	0.129	0.099	0.343	0.106	0.077
B	0.259	0.138	0.089	0.356	0.101	0.073
0.0316 mg/kg						
A	0.271	0.255	0.114	0.361	0.084	0.062
B	0.256	0.188	0.094	0.326	0.085	0.064
0.1 mg/kg						
A	0.417	0.794	0.149	0.411	0.066	0.047
B	0.217	0.240	0.113	0.370	0.069	0.051
0.316 mg/kg	0.662	2.228	0.120	0.215	0.034	0.030
1.0 mg/kg	0.102	0.435	0.074	0.592	0.015	0.017

Net uptake rate constants K_i were calculated from estimated parameter values as $(K_1k_3)/(k_2 + k_3)$.

be analyzed in a straightforward and robust manner using conventional kinetic analysis methods.

Isolated rat heart studies demonstrated that NET transports ^{11}C-GMO at a rate about 8 times slower than ^{11}C-HED (Fig. 3A). Similarly, NET transport assays using a rat C6 glioma cell line stably transfected with the cloned human NET (C6-hNET cells) showed that ^{11}C-GMO was transported at a rate about 9 times slower than ^{11}C-HED (*18*). We believe that this large reduction in the NET transport rate reduces the rate constant k_3 in the compartmental model to a magnitude that is less than k_2 (Fig. 1B). When $k_3 < k_2$, the tracer's net tissue uptake is not confounded by flow-limitation effects. As shown in Table 2, for all studies performed, k_3 was estimated to be less than k_2, which is consistent with the hypothesis that the net neuronal uptake of ^{11}C-GMO is not flow-limited. Thus we believe that the quantitative parameters K_i and K_p are likely to be sensitive measures of regional cardiac nerve density, capable of detecting mild-to-moderate nerve losses earlier in the progression of denervation than is currently possible with flow-limited tracers such as ^{11}C-HED or ^{123}I-MIBG. The dose–response curves shown in Figures 6E and 7B support this contention. Desipramine-induced declines in both K_i and K_p were well described by a sigmoidal dose–response model, with $r^2 > 0.99$ in each case. This means that more than 99% of the total variance in the net influx constants (K_i, K_p) is explained by variation in the desipramine dose (as modeled by the dose–response function), demonstrating the high sensitivity of these measures.

Not surprisingly, there was a high correlation between K_i and K_p, which are essentially 2 measures of the same aggregate combination of the model rate constants, $(K_1k_3)/(k_2 + k_3)$. In most cases, Patlak slopes K_p were a little lower than their corresponding K_i values. For Patlak analysis, we did not make any corrections to the tissue kinetics for the presence of radioactivity in blood vessels or for spillover effects between blood pool and myocardium. This resulted in a modest downward bias in the Patlak slopes. The compartmental model's *BV* parameter corrects for blood-borne radioactivity in tissue and for spillover effects (*19*). Although K_p was lower than K_i for most studies, for the highest desipramine concentration (1.0 mg/kg), K_p was higher than K_i (0.17 mL/min/g vs. 0.15 mL/min/g, respectively; Table 2). In this study, tissue activity levels were actually lower than blood activity levels late in the study, leading to a higher than average *BV* estimate, reflecting net spillover from blood into tissue. It appears that the compartmental modeling approach appropriately accounts for blood volume and spillover effects, and thus the calculated K_i constant should be more accurate than the Patlak slopes. That said, both measures are seen to provide an excellent index of NET transport rate.

We postulated that the main factor causing quantitative analyses of a tracer such as ^{11}C-HED to fail was its rapid NET transport rate, resulting in flow-limited uptake. The present results demonstrate that the slower NET transport rate of ^{11}C-GMO, combined with its efficient trapping in storage vesicles, leads to myocardial kinetics that can be analyzed successfully. However, it is possible that another factor may contribute to successful analysis of ^{11}C-GMO kinetics—the tendency of the tracer to stay in plasma throughout the study, with little trapping in RBCs, allowing intact ^{11}C-GMO molecules in plasma to accumulate slowly into nerve terminals during the entire PET study. ^{11}C-HED on the other hand tends to equilibrate with RBCs, reaching a C_p/C_{wb} ratio of 1.0 several minutes after tracer injection (*20*). If ^{11}C-HED molecules associated with RBCs are unavailable for extraction into tissue, preventing further accumulation into neurons, this may explain in part why cardiac ^{11}C-HED levels do not climb significantly after the rapid cardiac uptake seen early in a PET study (*21*). The uptake of ^{11}C-HED into RBCs may simply be due to passive diffusion, because it is more lipophilic than ^{11}C-GMO. However, the biogenic amines dopamine, norepinephrine, and epinephrine are all actively transported into RBCs (*22*), so it is possible that this mechanism is also involved.

jnm120659-pm ■ 7/22/13

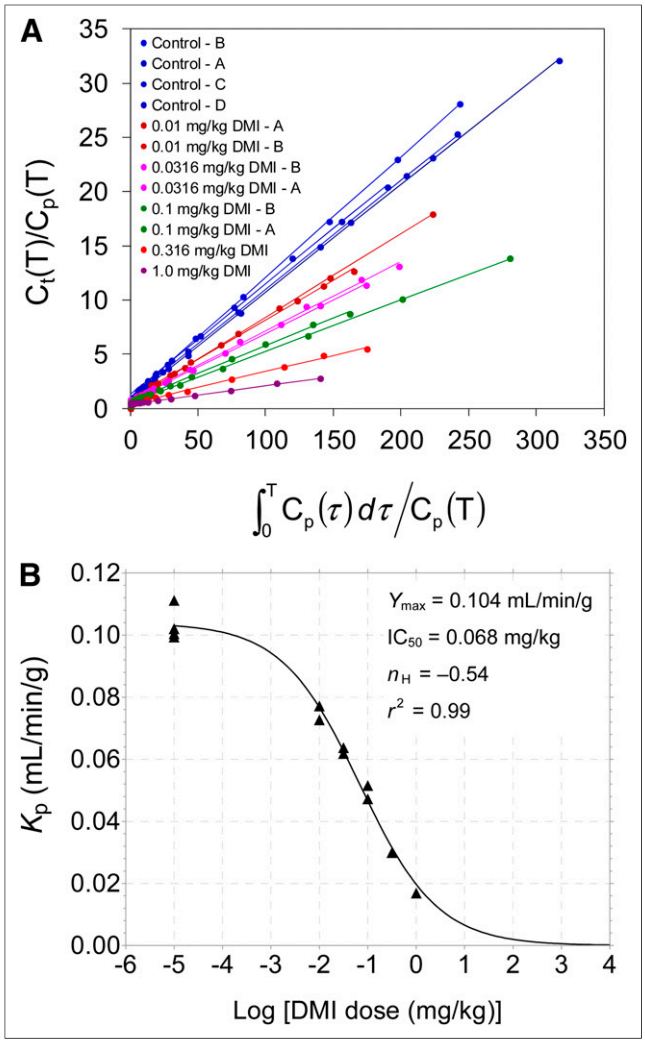

RGB

FIGURE 7. (A) Patlak plots of ^{11}C-GMO kinetics for all studies. Legend values are listed in order of highest Patlak slope to lowest, corresponding to values given in Table 2. (B) Relationship between Patlak slopes K_p (mL/min/g) and log [desipramine dose (mg/kg)]. Reductions in measured K_p values vs. desipramine dose were again well described by sigmoidal dose–response curve with variable Hill slope (n_H). Estimated parameter values for dose–response curve are shown.

Measurement of Regional Norepinephrine Uptake Rates

In cardiac PET studies of glucose metabolism with ^{18}F-FDG, it has been shown that regional metabolic rates of glucose utilization rMR_{glu} (μmol/min/g) can be calculated from net uptake rate constants K_i (or measured Patlak slopes K_p) (*23*). For such calculations, it is necessary to know the value of the lumped constant (LC) in the heart (the correction factor that relates the observed ^{18}F-FDG kinetics to those of glucose) and the subject's plasma glucose concentration C_{glu} (μmol/mL). Then rMR_{glu} can be calculated as:

$$rMR_{glu}\ (\mu mol/min/g) = K_i(mL/min/g) \times \frac{C_{glu}(\mu mol/mL)}{LC}. \quad \text{Eq. 4}$$

In a similar fashion, it may be possible to use regional K_i values from compartmental modeling of ^{11}C-GMO kinetics (or Patlak slopes K_p) to noninvasively estimate regional norepinephrine (NE) uptake rates (rUR_{NE}) in the heart, in units of pmol NE/min/g. This would require knowledge of the relative NET transport rates of norepinephrine and ^{11}C-GMO, here termed a relative transport constant $TC = UR_{GMO}/UR_{NE}$. In addition, the plasma concentration of norepinephrine C_{NE} (pmol NE/mL) would need to be measured for the subject. Then rUR_{NE} could be calculated as:

$$rUR_{NE}\ (pmol\ NE/min/g) = K_i(mL/min/g) \times \frac{C_{NE}(pmol\ NE/mL)}{TC}. \quad \text{Eq. 5}$$

As a starting point, TC can be approximated from isolated rat heart kinetics. In this system, ^{11}C-GMO has a NET-mediated uptake rate constant K_{up} equal to 0.30 mL/min/g (*8*), whereas the value for ^{3}H-norepinephrine is 4.44 mL/min/g (*24*), so that TC = 0.30/4.44 = 0.068. Plasma norepinephrine levels C_{NE} for female rhesus macaques held in captivity have been reported to be approximately 1.2 pmol/mL (*25*). Using K_i = 0.130 mL/min/g for ^{11}C-GMO, we can estimate rUR_{NE} in the rhesus macaque heart as:

$$rUR_{NE}\ (pmol\ NE/min/g) = (0.130\ mL/min/g) \times \frac{(1.2\ pmol/mL)}{0.068} = 2.3\ pmol/min/g$$

Values for comparison are difficult to find, but Eisenhofer et al. estimated a whole-heart UR_{NE} = 819 pmol/min in the human heart using ^{3}H-norepinephrine spillover techniques (*26*). Taking a nominal mass of 300 g for a normal adult human heart, an estimated regional rUR_{NE} value would be (819 pmol/min)/(300 g) = 2.7 pmol/min/g. These 2 estimates of rUR_{NE} agree well enough to suggest that this approach may provide a noninvasive method of measuring regional norepinephrine uptake rates in human subjects. Further work is needed to validate this approach. Although such measurements might not find routine clinical use, they may find application in clinical studies of the effects of diseases on regional norepinephrine reuptake rates or on the efficacies of drug therapies designed to improve or otherwise modulate norepinephrine reuptake rates.

CONCLUSION

^{11}C-GMO appears to be the first cardiac sympathetic nerve tracer possessing kinetics that can be analyzed in a straightforward manner to provide robust and sensitive quantitative measures of regional cardiac sympathetic nerve density. These quantitative measures will likely be able to detect mild-to-moderate sympathetic nerve losses that occur early in the course of cardiac denervation, which is not possible with existing tracers such as ^{11}C-HED and ^{123}I-MIBG. In addition, ^{11}C-GMO may find application in monitoring the efficacy of novel drug therapies designed to halt or reverse cardiac denervation in diseases associated with enhanced risk of sudden cardiac death, such as diabetic autonomic neuropathy and heart failure. Finally, it may be possible to noninvasively quantify regional norepinephrine reuptake rates through extension of the methodology currently used for measuring glucose metabolic rates from parameters measured from ^{18}F-FDG kinetics.

jnm120659-pm ■ 7/22/13

DISCLOSURE

The costs of publication of this article were defrayed in part by the payment of page charges. Therefore, and solely to indicate this fact, this article is hereby marked "advertisement" in accordance with 18 USC section 1734. This work was supported by PHS grant R01-HL079540 from the National Heart Lung and Blood Institute, National Institutes of Health, Bethesda, MD. No other potential conflict of interest relevant to this article was reported.

ACKNOWLEDGMENT

We thank the staff of the University of Michigan Cyclotron Facility for preparing ^{11}C-HED and ^{18}F-FDG.

REFERENCES

1. Raffel DM, Wieland DM. Development of mIBG as a cardiac innervation imaging agent. *JACC Cardiovasc Imaging.* 2010;3:111–116.
2. Bengel FM. Imaging targets of the sympathetic nervous system of the heart: translational considerations. *J Nucl Med.* 2011;52:1167–1170.
3. Henneman MM, Bengel FM, van der Wall EE, Knuuti J, Bax JJ. Cardiac neuronal imaging: application in the evaluation of cardiac disease. *J Nucl Cardiol.* 2008;15:442–455.
4. Boogers MJ, Fukushima K, Bengel FM, Bax JJ. The role of nuclear imaging in the failing heart: myocardial blood flow, sympathetic innervation, and future applications. *Heart Fail Rev.* 2011;16:411–423.
5. Raffel DM, Wieland DM. Assessment of cardiac sympathetic nerve integrity with positron emission tomography. *Nucl Med Biol.* 2001;28:541–559.
6. Raffel DM. Targeting norepinephrine transporters in cardiac sympathetic nerve terminals. In: Welch MJ, Eckelman WC, eds. *Targeted Molecular Imaging*. Boca Raton, FL: CRC Press; 2012:305–320.
7. Patlak CS, Blasberg RG. Graphical evaluation of blood-to-brain transfer constants from multiple-time uptake data: generalizations. *J Cereb Blood Flow Metab.* 1985;5:584–590.
8. Raffel DM, Jung YW, Gildersleeve DL, et al. Radiolabeled phenethylguanidines: novel imaging agents for cardiac sympathetic neurons and adrenergic tumors. *J Med Chem.* 2007;50:2078–2088.
9. Rosenspire KC, Haka MS, Van Dort ME, et al. Synthesis and preliminary evaluation of carbon-11-meta-hydroxyephedrine: a false transmitter agent for heart neuronal imaging. *J Nucl Med.* 1990;31:1328–1334.
10. Richards ML, Scott PJH. Synthesis of [^{18}F]fluorodeoxyglucose ([^{18}F]FDG). In: Scott PJH, Hockley BG, eds. *Radiochemical Syntheses Volume 1: Radiopharmaceuticals for Positron Emission Tomography.* Hoboken, NJ: John Wiley & Sons; 2012:3–13.
11. National Research Council. *Guide for the Care and Use of Laboratory Animals.* Bethesda, MD: U.S. Department of Health and Human Services, National Institutes of Health; 1985.
12. Taegtmeyer H, Hems R, Krebs HA. Utilization of energy providing substrates in the isolated working rat heart. *Biochem J.* 1980;186:701–711.
13. Raffel D, Loc'h C, Mardon K, Mazière B, Syrota A. Kinetics of the norepinephrine analog [Br-76]-*meta*-bromobenzylguanidine in isolated working rat heart. *Nucl Med Biol.* 1998;25:1–16.
14. Tai C, Chatziioannou A, Siegel S, et al. Performance evaluation of the microPET P4: a PET system dedicated to animal imaging. *Phys Med Biol.* 2001;46:1845–1862.
15. Qi J, Leahy RM. Resolution and noise properties of MAP reconstruction for fully 3D-PET. *IEEE Trans Med Imaging.* 2000;19:493–506.
16. Kuntzman R, Jacobson MM. Monoamine oxidase inhibition by a series of compounds structurally related to bretylium and guanethidine. *J Pharmacol Exp Ther.* 1963;141:166–172.
17. Ratib O, Phelps ME, Huang SC, Henze E, Selin CE, Schelbert HR. Positron tomography with deoxyglucose for estimating local myocardial glucose metabolism. *J Nucl Med.* 1982;23:577–586.
18. Raffel DM, Chen W, Jung YW, Jang KS, Gu G, Cozzi NV. Radiotracers for cardiac sympathetic innervation: transport kinetics and binding affinities for the human norepinephrine transporter. *Nucl Med Biol.* 2013;40:331–337.
19. Hutchins GD, Schwaiger M, Rosenspire KC, Krivokapich J, Schelbert H, Kuhl DE. Noninvasive quantification of regional blood flow in the human heart using N-13 ammonia and dynamic positron emission tomographic imaging. *J Am Coll Cardiol.* 1990;15:1032–1042.
20. Law MP, Osman S, Davenport RJ, Cunningham VJ, Pike VW, Camici PG. Biodistribution and metabolism of [N-methyl-^{11}C]-*m*-hydroxyephedrine in the rat. *Nucl Med Biol.* 1997;24:417–424.
21. Raffel DM, Corbett JR, del Rosario RB, et al. Clinical evaluation of carbon-11-phenylephrine: MAO sensitive marker of cardiac sympathetic neurons. *J Nucl Med.* 1996;37:1923–1931.
22. Azoui R, Cuche J-L, Renaud J-F, Safar M, Dagher G. A dopamine transporter in human erythrocytes: modulation by insulin. *Exp Physiol.* 1996;81:421–434.
23. Gambhir SS, Schwaiger M, Huang SC, et al. Simple noninvasive quantification method for measuring myocardial glucose utilization in humans employing positron emission tomography and fluorine-18 deoxyglucose. *J Nucl Med.* 1989;30:359–366.
24. Iversen LL. Role of transmitter uptake mechanisms in synaptic neurotransmission. *Br J Pharmacol.* 1971;41:571–591.
25. Lilly AA, Mehlman PT, Higley JD. Trait-like immunological and hematological measures in female rhesus across varied environmental conditions. *Am J Primatol.* 1999;48:197–223.
26. Eisenhofer G, Esler MD, Meredith IT, et al. Sympathetic nervous function in human heart as assessed by cardiac spillovers of dihydroxyphenylglycol and norepinephrine. *Circulation.* 1992;85:1775–1785.